Pergamon

Geochimica et Cosmochimica Acta, Vol. 67, No. 15, pp. 2749–2761, 2003

0016-7037/03 $30.00 + .00

doi:10.1016/S0016-7037(03)00097-8

Geochemical reactions and dynamics during titration of a contaminated groundwater with high uranium, aluminum, and calcium

BAOHUA GU,* SCOTT C. BROOKS, YUL ROH, and PHILIP M. JARDINE
Environmental Sciences Division, Oak Ridge National Laboratory, P.O. Box 2008, Oak Ridge, TN 37831

(*Received July* 10, 2002; *accepted in revised form January* 16, 2003)

Abstract—This study investigated possible geochemical reactions during titration of a contaminated groundwater with a low pH but high concentrations of aluminum, calcium, magnesium, manganese, and trace contaminant metals/radionuclides such as uranium, technetium, nickel, and cobalt. Both Na-carbonate and hydroxide were used as titrants, and a geochemical equilibrium reaction path model was employed to predict aqueous species and mineral precipitation during titration. Although the model appeared to be adequate to describe the concentration profiles of some metal cations, solution pH, and mineral precipitates, it failed to describe the concentrations of U during titration and its precipitation. Most U (as uranyl, UO_2^{2+}) as well as Tc (as pertechnetate, TcO_4^-) were found to be sorbed and coprecipitated with amorphous Al and Fe oxyhydroxides at pH below ~5.5, but slow desorption or dissolution of U and Tc occurred at higher pH values when Na_2CO_3 was used as the titrant. In general, the precipitation of major cationic species followed the order of $Fe(OH)_3$ and/or $FeCo_{0.1}(OH)_{3.2}$, $Al_4(OH)_{10}SO_4$, $MnCO_3$, $CaCO_3$, conversion of $Al_4(OH)_{10}SO_4$ to $Al(OH)_{3,am}$, $Mn(OH)_2$, $Mg(OH)_2$, $MgCO_3$, and $Ca(OH)_2$. The formation of mixed or double hydroxide phases of Ni and Co with Al and Fe oxyhydroxides was thought to be responsible for the removal of Ni and Co in solution. Results of this study indicate that, although the hydrolysis and precipitation of a single cation are known, complex reactions such as sorption/desorption, coprecipitation of mixed mineral phases, and their dissolution could occur simultaneously. These processes as well as the kinetic constraints must be considered in the design of the remediation strategies and modeling to better predict the activities of various metal species and solid precipitates during pre- and post-groundwater treatment practices. *Copyright © 2003 Elsevier Ltd*

1. INTRODUCTION

Past waste disposal activities at the U.S. Department of Energy's (DOE) Oak Ridge Y-12 S-3 site have created a mixed-waste plume of contamination in the underlying unconsolidated residuum and competent shale bedrock. The plume is more than 400 ft deep directly beneath the ponds and extends ~4000 ft along geologic strike both east and west of the ponds. The S-3 site consisted of four unlined ponds constructed in 1951 and had a storage capacity of ~10 million gallons. Liquid wastes, composed primarily of nitric acid plating wastes, containing various metals and radionuclides (e.g., U, Ni, and Tc) were disposed of in the ponds until 1983. Volatile organic compounds such as tetrachloroethylene and acetone also were disposed in the ponds and detected in the groundwater near the ponds. The groundwater plume is stratified, with the distribution of contaminants dependent on geochemical properties of contaminants themselves and the groundwater flow. In other words, heavy metals such as Ni and U that are more reactive with soil and sediment minerals have not migrated as extensively away from the ponds as some anionic species. On the other hand, nitrate and pertechnetate (TcO_4^-), which are not particularly reactive with soil minerals, have the most extensive distribution in groundwater (Cook et al., 1996; Gu et al., 2002).

Remedial activities have been ongoing since 1984, when pond wastes were partially neutralized and denitrified, and the site was capped and paved thereafter (Cook et al., 1996; SAIC, 1997). Investigations have also been performed to study the potential for removal of radioactive uranium U(VI) and technetium Tc(VII) species as well as high nitrate in groundwater, such as the application of permeable iron reactive barrier (Gu et al., 1998; 2002) and in situ bioremediation technologies supported by DOE environmental management and the Natural and Accelerated Bioremediation Research (NABIR) program (http://www.lbl.gov/NABIR). This work was carried out as part of a larger study involving the in situ immobilization of U(VI) and Tc(VII) by microbial reduction of these elements to sparingly soluble U(IV) and Tc(IV) species. This may be accomplished by delivery of electron donors and nutrients to the subsurface so as to stimulate the growth of indigenous anaerobic microorganisms and thus to reduce U(VI) and Tc(VII) during microbial respiration processes (Lovley, 1995; Fredrickson and Gorby, 1996; Fredrickson et al., 2000; Wildung et al., 2000). However, preliminary analyses indicate that factors other than electron donor/nutrient availability are limiting or inhibiting microbial growth at the site, and these factors include a low pH and high concentrations of toxic metals and/or cocontaminants such as Al, Ni, and nitrate (Table 1). Pretreatment of groundwater such as base titration is thus necessary to increase the groundwater pH and reduce the levels of some toxic metals by precipitation in order for microorganisms to grow.

Although the hydrolysis and precipitation of individual metals or radionuclides found in this groundwater are known and well documented (Baes and Mesmer, 1976; Bibak et al., 1995; Towle et al., 1997), such behavior could be complex when dealing with a contaminated groundwater involving multiple cationic and anionic species with a wide range of concentrations (Table 1). The precipitation, coprecipitation, sorption,

* Author to whom correspondence should be addressed (gub1@ornl.gov).

Table 1. Major constituents found in groundwater near the Oak Ridge Y-12 S-3 Ponds (sampled from monitoring well FW-026 on May 30, 2001). Groundwater pH is ~3.7.

Constituents	Concentration (mg/L)	Constituents	Concentration (mg/L)
Al	453	U	50.5
Ca	955	Tc	1.6×10^{-3}
Co	2.3	NO_3^-	7950
Fe	13.6	SO_4^{2-}	982
Mg	160	CI^-	88
Mn	129	TOC	64
Ni	12.5	TIC	240
K	93	DO	2–4
Si	24		

TOC = total organic carbon; TIC = total inorganic carbon; DO = dissolved oxygen.

desorption, and dissolution may occur simultaneously as groundwater pH changes, and such processes could not be predicted by the pure phase solubility products (K_{sp}) of corresponding minerals. To simulate the field groundwater titration or neutralization process, the present work was therefore undertaken to determine aqueous-solid phase compositional changes and equilibrium (e.g., precipitation and dissolution, and adsorption and desorption) during the base titration. This effort coupled with geochemical modeling was designed to better predict dissolved metal/radionuclide activities at pre/posttitration conditions and may lead us to perform more successful bioremediation at the site.

2. MATERIAL AND METHODS

2.1. Site Groundwater and Solution Analysis

The groundwater samples used for the titration experiment were obtained from the monitoring well FW-026 at the NABIR field research center (FRC) at the Y-12 National Security Plant site in Oak Ridge, Tennessee. In general, the groundwater is characterized with high levels of Ca^{2+}, Al^{3+}, NO_3^-, and SO_4^{2-} with major contaminant metals including uranium, nickel, and technetium (Table 1). Both uranium and technetium are radioactive and, under oxic conditions such as those at the S-3 site, they are anticipated to be present in groundwater in forms of uranyl (UO_2^{2+}) and pertechnetate (TcO_4^-) (Langmuir, 1978; Gu et al., 2000). However, because of relatively high groundwater concentrations of carbonate (generated from acidic dissolution of limestone residuum in the subsurface media), dissolved O_2 (DO), nitrate, and SO_4^{2-}, uranyl may also be present in groundwater as uranyl carbonates (e.g., UO_2CO_3 and $UO_2(CO_3)_2^{2-}$), nitrates (e.g., $UO_2NO_3^+$), and/or sulfates (UO_2SO_4, $UO_2(SO_4)_2^{2-}$) (Couston et al., 1995; Moulin et al., 1998).

An inductively coupled plasma (ICP)–atomic emission spectrophotometer (Thermo Jarrell Ash PolyScan Iris Spectrometer) was used for the total dissolved elemental analysis (such as Al, Ca, Co, Fe, Mg, Mn, Ni, K, and Si), whereas an ion chromatograph (Dionex DX-500) was used for the analysis of common anions (e.g., NO_3^-, Cl^-, and SO_4^{2-}) using Dionex AS4A and AG4A analytical columns (Gu et al., 2002). The total inorganic carbon (TIC) was determined by purging acidified groundwater with high-purity O_2, and the nonpurgeable total organic carbon (TOC) was determined by the high-temperature combustion using a Shimadzu 5000A Carbon analyzer (Gu et al., 2002). Technetium-99 was assayed by liquid scintillation counting, and uranium was analyzed by the steady-state phosphorescence techniques, as were reported previously (Kaminski et al., 1981; Brina and Miller, 1992; Gu et al., 2002). All U measurements were performed using a Fluorolog-3 fluorescence spectrometer equipped with both excitation and emission monochromators (Johin-Yvon-SPEX instruments, Edison, New Jersey). A 450-W Xenon arc lamp was used as the excitation source, and the emission spectra were collected from 482 to 555 nm with an excitation wavelength at 280 nm. The peak emission at 515.4 nm was used for the calculation of U(VI) phosphorescence intensity or U(VI) concentration in solution.

2.2. Titration Experiment

Titration of the contaminated groundwater was performed in batch experiments to evaluate the dynamics of the precipitation and/or dissolution/desorption of contaminant metals and radionuclides under varying pH conditions. Because of the production of carbonate or bicarbonate species during microbial respiration, both NaOH and Na_2CO_3 were used for the titration and studied for their effects on the precipitation and/or coprecipitation of metal/radionuclide contaminants. Literature data (Scheidegger et al., 1998; Thompson et al., 1999; Bargar et al., 2000) and preliminary experiments indicate that the dynamics of the precipitation, dissolution, adsorption, and desorption of some metals and radionuclides and their oxyhydroxides require a rather long equilibrium time (days or months) after addition of the base. However, for this laboratory simulated titration experiment, a two-day equilibrium time was used after mixing the contaminated groundwater with the base at varying pH conditions. Briefly, the contaminated groundwater (20 mL) was placed in a series of polyethylene vials, to which various amounts (0–1.2 mL) of either 2 mol/L NaOH or Na_2CO_3 were added to give a pH range from ~3.8 to 9. The final volume was made up to 21.2 mL for all samples. The sample vials were then placed on an end-over-end shaker for 2 d, and the final pH was measured by means of a precalibrated pH potentiometer (Model 920A, Orion Research Inc.). An aliquot of sample (or suspension) was filtered with a 0.2-μm polytetrafluoroethylene (PTFE) syringe filter, and the clear supernatant solution was analyzed for soluble metals (e.g., Al, Fe, Ca, Mg, Mn, Co, Ni, Si, K), radionuclides (U and Tc), and common anions (e.g., SO_4^{2-}, NO_3^-, and Cl^-), as described earlier. Some selected samples were duplicated, and analytical errors were estimated to be about ±10%, considering possible interferences and dilutions necessary for the analysis of groundwater constituents in a wide concentration range (Table 1). It should also be pointed out that a small headspace (~4.3 mL) was left in sample vials, and the titration was not performed under anaerobic conditions because of a relatively high DO content in the initial groundwater (Table 1). Additionally, CO_2 was not excluded in the NaOH experimental system although the system might not be equilibrated with the atmosphere either because of a limited headspace.

Selected groundwater samples were also prepared to evaluate the kinetic changes in pH and U and Tc concentrations

Table 2. Solid phases considered in the reaction path model.

Reaction	log K	
$Al(OH)_{3,am} + 3H^+ = Al^{3+} + 3H_2O$	10.8	(a)
$Al_4(OH)_{10}SO_4 + 10H^+ = 4Al^{3+} + SO_4^{2-} + 10H_2O$	25	(b)
$FeCo_{0.1}(OH)_{3.2} + 3.2H^+ = Fe^{3+} + 0.1Co^{2+} + 3.2H_2O$	5.7	(b)
$MnCO_{3,syn} + H^+ = Mn^{2+} + HCO_3^-$ (synthetic rhodochrosite)	−0.061	(a)
$CaMg(CO_3)_2 + 2H^+ = Ca^{2+} + Mg^{2+} + 2HCO_3^-$ (disordered dolomite)	4.118	(a)
$UO_2CO_3 + H^+ = UO_2^{2+} + HCO_3^-$	−4.143	(c)
$CaUO_4 + 4H^+ = Ca^{2+} + UO_2^{2+} + 2H_2O$	15.931	(c)
$UO_3 \cdot 2H_2O + 2H^+ = UO_2^{2+} + 3H_2O$ (schoepite)	4.812	(c)
β-$UO_2(OH)_2 + 2H^+ = UO_2^{2+} + H_2O$	4.93	(c)
$CaCO_3 \cdot H_2O + H^+ = Ca^{2+} + HCO_3^- + H_2O$ (monohydrocalcite)	2.729	(d)
$Ca_{0.85}Mg_{0.15}CO_3 + H^+ = 0.85Ca^{2+} + 0.15Mg^{2+} + HCO_3^-$ (magnesian calcite)	2.9	(e)
$Ni(OH)_2 + 2H^+ = Ni^{2+} + 2H_2O$	10.8	(f)
$Co(OH)_2 + 2H^+ = Co^{2+} + 2H_2O$	12.1	(f)
$NiCO_3 + H^+ = Ni^{2+} + HCO_3^-$	3.512	(g)
$CoCO_3 + H^+ = Co^{2+} + HCO_3^-$	−0.233	(h)

[a] Nordstrom et al., 1990.
[b] Estimated for this study.
[c] Grenthe et al., 1992.
[d] Hull and Turnbull, 1973.
[e] Interpolated from data of Plummer and MacKenzie (1974) as shown in Figure 1 of Bischoff et al. (1987).
[f] Baes and Mesmer, 1976.
[g] Wagman et al., 1982.
[h] Sverjensky, 1984.

during the 2-d titration period. Briefly, one hundred milliliters of groundwater were first added with a fixed amount of 2 mol/L Na_2CO_3 to a pseudo-equilibrium pH (~7.5) in a short time period (i.e., a pH value was read in ~5 min after addition of the base). The sample was then placed on a shaker, and an aliquot of sample was taken periodically but analyzed immediately for pH. The U and Tc concentrations were determined after samples were filtered with a 0.2-μm PTFE syringe filter as described earlier.

2.3. Mineralogical Characterization of Precipitated Solids

The precipitated solids for some selected samples during titration were analyzed for mineralogical characteristics by means of a Scintag XDS 2000 X-ray diffractometer (XRD) operated at 40 kV and 35 mA (Scintag, Inc. Sunnyvale, CA). The filtered precipitates were first air-dried at room temperature and then transferred onto a glass slide for the XRD analysis. The scan rate was 2° 2θ/min using Co-Kα radiation (λ = 0.17889 nm). In addition, a scanning electron microscope (SEM) equipped with an energy dispersive X-ray (EDX) detector (JEOL JSM-35CF, Tokyo, Japan) was used for the analysis of morphology and surface elemental composition of the precipitated minerals (Gu et al., 2002).

2.4. Geochemical Process Model of Titration

The geochemical processes governing changes in the solution composition during the titration were simulated by a reaction path model using the REACT module in the commercially available software program The Geochemist's Workbench (Bethke, 2001). The program was used to calculate the isothermal equilibrium distribution of elements between aqueous and solid phases. Because of a low initial groundwater pH (~3.8), dissolved metal cations such as Al^{3+}, Fe^{3+}, Ca^{2+}, Mg^{2+}, Mn^{2+}, Co^{2+}, Ni^{2+}, and K^+ were presumably the predominant aqueous species in groundwater. The Fe(II) concentration was also assumed to be low or negligible because of a low total Fe concentration but a relatively high DO concentration in groundwater (Table 1). The initial system consisted of 1 kg water with a composition constrained by the groundwater analysis and was then titrated with either NaOH or Na_2CO_3. The model assumed the titration system to be closed to the atmosphere, i.e., we did not assume equilibrium with atmospheric CO_2. The NaOH titrant used in experiments was not CO_2-free, therefore, the model assumed the NaOH to contain 0.07 mol of total carbonate per mole NaOH. The simulation results reflect how the equilibrated system (aqueous species plus mineral assemblage) changes over the course of the titration. The Lawrence Livermore National Laboratories database (Delany and Lundeen, 1990) was used with modifications as noted. Thermodynamic data for U were verified against the extensive compilation of Grenthe et al. (1992). The calculated ionic strength of the solutions were all less than 0.21, thus the activity coefficients were calculated using the extended Debye-Huckel equation.

In addition to precipitation, sorption onto the variable charge surfaces of Fe and Al hydroxides was also considered as a mechanism exerting control on the concentration of metals in solution. Sorption reactions for $Fe(OH)_{3,am}$ (or ferrihydrite) were implemented following the model described by Dzombak and Morel (1990). A similar set of reactions was included for the sorption of Co, Ni, and U onto Al hydroxide surfaces.

2.5. Constraints on the Solid-phase Assemblage

The initial water composition was oversaturated with respect to a large number of crystalline solids. We therefore assumed the initial water to be metastable with respect to those solids and that precipitation was dependent on perturbing the system

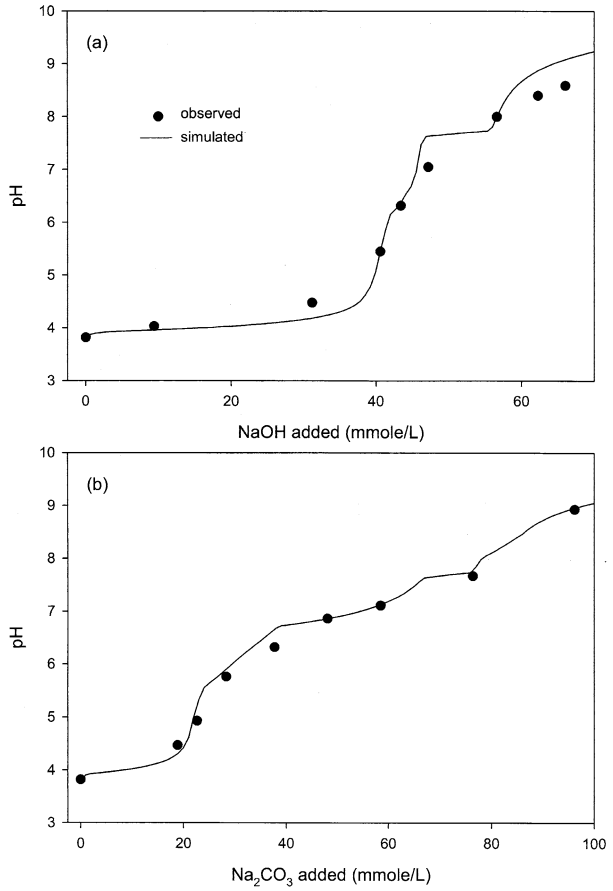

Fig. 1. Observed and simulated solution pH as a function of titrant addition with: (a) NaOH and (b) Na_2CO_3.

via base addition. In addition, X-ray diffraction analysis indicated that the precipitated solids were dominated by amorphous or poorly crystalline materials. The solid phases considered for the reaction path model simulation are listed in Table 2.

3. RESULTS AND DISCUSSION

Titration of the acidic groundwater with either NaOH or Na_2CO_3 showed broad regions of buffering, reflecting the complex nature of the sample and suggesting that multiple reactions are responsible for the buffering action (Fig. 1a,b). The initial stages of titration with either titrant were similar; the pH was resistant to change until more than 32 mmol/L of NaOH or ~16 mmol/L of Na_2CO_3 (~32 meq/L of base) were added. Nevertheless, the remaining portions of the titrations were distinctly different. The pH increased from 4.5 to 8.6 with an additional 35 mmol/L NaOH added, whereas an additional ~77 mmol/L (or ~154 meq/L) Na_2CO_3 were required to effect a similar pH change. The reaction path model did an adequate job describing the titration curves (Fig. 1a,b, solid lines). The specifics of the pH buffering reactions and changes in solution composition are discussed in detail in the following sections.

3.1. Geochemical Reactions and Mineral Precipitation in Hydroxide System

3.1.1. Al, Fe, and SO_4^{2-} Concentrations

The concentration profiles of major cations, radionuclides, and SO_4^{2-} during titration of groundwater with NaOH are presented in Figure 2. As expected, addition of NaOH resulted in first the precipitation of Al and Fe hydroxide minerals (Fig. 2a,b) because of their relatively low solubility. Most Fe was precipitated out at pH above ~4.5 (or with ~32 mmol/L NaOH added). The model seems to have overestimated the Fe concentration in solution, probably because of its coprecipitation with Al hydroxides. The total Fe concentration is only a small a fraction (~3%) of Al, which is one of the major cations in groundwater (Table 1). Therefore, in the first part of the titration, solution pH should be largely buffered by the hydrolysis of Al (and Fe to a lesser extent) resulting in the formation of aqueous hydrolysis species as well as the solid-phase precipitates. Most of the Al was precipitated out when the solution pH was raised to ~5 (or with ~40 mmol/L NaOH added), and only negligible amounts of Al were left in the solution phase. Although to a lesser extent, a noticeable decrease in the SO_4^{2-} concentration was also observed. These observations might suggest the coprecipitation of mixed solid phases into which were incorporated cations other than Fe or Al and counterions other than OH^- in the early stages of the titration with <40 mmol/L NaOH added (Fig. 2a,b).

To investigate possible controls on Al^{3+} activity ($\{Al^{3+}\}$) during titration, activity ratio diagrams were constructed by considering $Al(OH)_{3,am}$ and an Al-OH-SO_4 solid phase (Fig. 3). Plots of the calculated activity of Al^{3+} and SO_4^{2-} vs. pH indicated a solid phase with SO_4:Al:OH ratio of 1:4:10 and a log K_{so} = 25, assuming the initial solution to be slightly undersaturated with respect to the solid. This value is in good agreement with amorphous basaluminite ($Al_4(OH)_{10}SO_{4,am}$) (Nordstrom, 1982). Amorphous basaluminite is a metastable solid phase but its precipitation is kinetically favored under the experimental conditions with relatively high Al and SO_4^{2-} concentrations. Several researchers have noted that basaluminite is the first solid phase to form upon titration of aluminum sulfate solutions, which subsequently alters to more stable phases under various conditions (Roberson and Hem, 1969; Adams and Rawajfih, 1977; Adams and Hajek, 1978). Based on these stoichiometries, the following relationships are developed:

$$Al(OH)_{3,am} + 3H^+ \Leftrightarrow Al^{3+} + 3H_2O \qquad \log K = 10.8$$

$$\log \frac{\{solid\}}{\{Al^{3+}\}} = 3\log\{H_2O\} + 3pH - \log K \qquad (1)$$

$$Al_4(OH)_{10}SO_4 + 10H^+ \Leftrightarrow 4Al^{3+} + SO_4^{2-} + 10H_2O \qquad \log K \approx 25$$

$$\log \frac{\{solid\}^{0.25}}{\{Al^{3+}\}} = 0.25\log\{SO_4^{2-}\} + 2.5pH + 2.5\log\{H_2O\} - 0.25\log K \qquad (2)$$

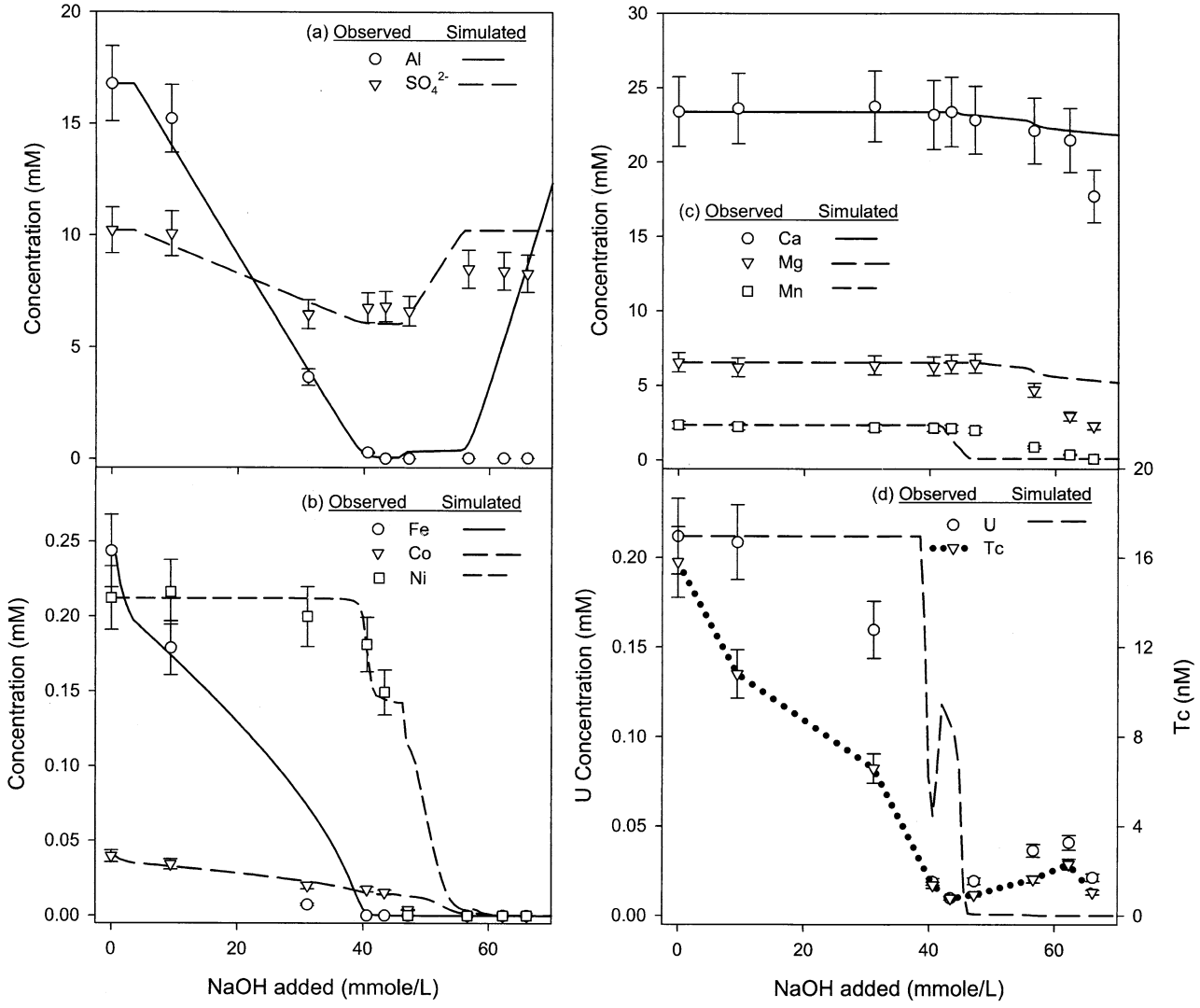

Fig. 2. Observed and simulated total concentrations of metal cations, Tc, and sulfate for the NaOH titration of a contaminated groundwater with a low pH and high concentrations of Al and Ca. Symbols represent observed data, whereas lines are model simulations except for Tc. Error bars indicate ±10% of the observed value.

The calculated water activity was greater than 0.99 for all titration points so we assumed $\{H_2O\} = \{\text{solid}\} = 1$ and that $\{SO_4^{2-}\}$ = average $\{SO_4^{2-}\}$ within each titration. The calculated $\{Al^{3+}\}$ plotted with the lines defined by Eqn. 1 and 2 indicate that $Al_4(OH)_{10}SO_4$ controls $\{Al^{3+}\}$ below pH 7.7 whereas $Al(OH)_{3,am}$ controls the activity of Al^{3+} at higher pH (Fig. 3a). These calculations provide support for the precipitation of a mixed Al-OH-SO_4 solid phase during the initial stages of the titration with alteration to $Al(OH)_{3,am}$ as the pH increased.

The simulated total concentrations of Al and SO_4^{2-} are in good agreement with the observations for titrant addition at <57 mmol/L NaOH (Fig. 2a). Sulfate concentrations increased as $Al_4(OH)_{10}SO_4$ altered to $Al(OH)_{3,am}$ with further addition of NaOH. The subsequent dissolution of the latter phase due to the amphoteric nature of Al resulted in increased Al concentrations in model simulations when addition of NaOH was >57 mmol/L. The observed concentrations of SO_4^{2-} did increase in the experiments but not to the extent seen in the simulation. This lack of agreement between model and observations at the higher pH may be due to kinetic effects of Al dissolution, which were not included in the model calculations. The measured dissolution rate of corundum (α-Al_2O_3) at room temperature in alkaline solution suggests that the 48-h equilibration period of these experiments was likely insufficient to reach equilibrium (Carroll-Webb and Walther, 1988). Although the concentration of Al in equilibrium with corundum at 25°C increases with pH > 5.8, the rate of dissolution in the pH range of 8–9 is ~10 times slower than at more acidic pH and up to 100 times slower than it is at more alkaline pH.

3.1.2. Co and Ni Concentrations

The close geochemical relationship between Fe and Co has long been recognized (Towle et al., 1997; Thompson et al., 1999). As shown in Figure 2b, solution Co^{2+} concentration

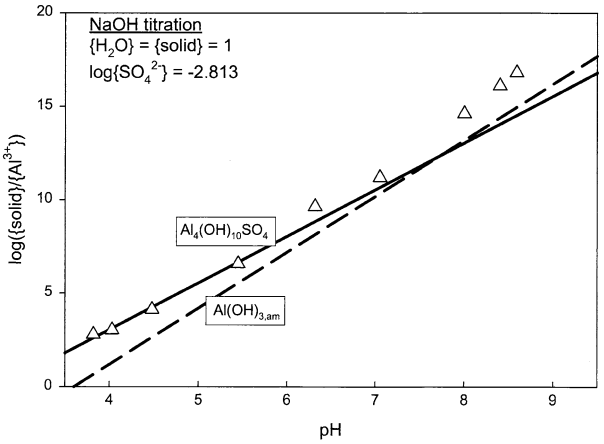

Fig. 3. Activity ratio diagrams for the titration of groundwater with either NaOH or Na_2CO_3. The results indicate that the activity of Al^{3+} is controlled by $Al_4(OH)_{10}SO_4$ at pH below 7.7 and $Al(OH)_{3,am}$ at higher pH.

decreased consistently along with Al and Fe during the titration (Fig. 2a,b). An analysis similar to that described for Al was also conducted for a possible Fe-Co-OH solid. The results suggested that a mixed solid of composition $FeCo_{0.1}(OH)_{3.2}$ with a log $K_{so} = 5.7$ exerted control on the $\{Fe^{3+}\}$ and $\{Co^{2+}\}$. There is greater uncertainty in this analysis, as there were only three data points, spanning a narrow pH range from ~3.8 to 4.5 (with ~32 mmol/L NaOH added), where there were detectable amounts of Fe^{3+}. The model accounted for Co^{2+} sorption onto Al oxyhydroxides, and this mechanism may be responsible for the remaining loss of Co^{2+} as basaluminite alters to $Al(OH)_{3,am}$ (Fig. 2b). Previous studies have shown that, in comparison with crystalline Fe-oxyhydroxides and phyllosilicate minerals, Al-oxyhydroxides are particularly effective in sorbing Co^{2+} by forming a double-hydroxide phase (Bibak et al., 1995; Towle et al., 1997). These colloidal precipitates or coprecipitates are particularly stable and less soluble than either $Al(OH)_3$ or $Co(OH)_2$ alone (Towle et al., 1997).

The concentration profile of Ni^{2+} was described well by the model (Fig. 2b), considering its sorption and precipitation of $Ni(OH)_2$. The concentration of Ni^{2+} remained relatively constant in the first part of the titration but decreased rapidly when titrant addition exceeded 40 mmol/L NaOH (or at pH above ~5) (Fig. 1) and appeared to be consistent with the alteration from $Al_4(OH)_{10}SO_4$ to $Al(OH)_{3,am}$ solid phases. In other words, the loss of Ni may be first caused by sorption onto basaluminite, followed by Ni sorption onto $Al(OH)_3$ as it forms from basaluminite. Note that the solution concentrations of Ca, Mn, and Mg remained relatively constant at pH $<$~6 (Fig. 2c), so that coprecipitation of $NiCO_3$ with $CaCO_3$ or $MnCO_3$ did not appear to be a plausible explanation. On the other hand, Ni^{2+} is known to be strongly sorbed by Al and Fe oxyhydroxides (Ticknor, 1994; Bibak et al., 1995; Scheidegger et al., 1997; Towle et al., 1997; Green-Pedersen and Pind, 2000). Green-Pedersen and Pind (2000) reported that the sorption of Ni on Fe-oxyhydroxides increased with both pH and solution concentration. It has been suggested that the sorption mechanism may involve a combination of ion exchange and surface complexation (Ticknor, 1994). More recently, analyses by X-ray absorption fine structure spectroscopy and X-ray photo spectroscopy indicated that sorption and coprecipitation of Ni and Al-oxyhydroxides occurred by forming a double-hydroxide phase with greatly increased stability with respect to dissolution (Towle et al., 1997; Scheckel et al., 2000).

3.1.3. Ca, Mg, and Mn Concentrations

The model simulation did well in describing the concentration profiles of Ca^{2+}, Mg^{2+}, and Mn^{2+} in the initial phase of the titration, but deviated from experimental observations when more than 40 mmol/L of NaOH was added (Fig. 2c). Less than 10% of Ca^{2+} was precipitated out with addition of ~60 mmol/L NaOH (or at pH ~8.5). A single $CaMg(CO_3)_2$ phase was adequate to describe Ca^{2+} and Mg^{2+} concentrations (Table 2, Fig. 2c). However, the model solution became oversaturated with $MnCO_3$, resulting in the precipitation of this solid phase starting at ~42 mmol/L of NaOH added (or at pH ~6.2). The experimental data indicate that Mn^{2+} loss from solution occurred at higher pH, coinciding with decreased concentrations of Ca and Mg suggesting either coprecipitation with or surface sorption onto Ca or Mg solids (Zachara et al., 1991). The deviation may also partially result from an overestimation of carbonate activity in solution because samples were neither purged nor equilibrated with atmospheric CO_2 ($P_{CO_2} = 10^{-3.5}$), as stated earlier.

3.1.4. U and Tc Concentrations

Uranium (U) and technetium (Tc) are the major contaminants of concern at the site. The oxidized forms of U(VI) are predominant in the groundwater as measured by fluorescence spectroscopy which is specific for the detection of hexavalent uranium (Gu et al., 2002). Similarly, pertechnetate (TcO_4^-) anions were considered the dominant species in groundwater. The fact that Tc is highly mobile at the site is indicative of its presence as TcO_4^- anionic species in groundwater. The measured U and Tc concentration profiles (and U model simulation) are shown in Figure 2d. The simulation did a poor job describing changes in U concentration, and the reaction path model did not consider TcO_4^-. The model predicts that UO_2^{2+} and $UO_2SO_{4,aq}$ are the dominant species up to ~42 mmol/L NaOH added (pH 5.5) above which precipitation of U as UO_2CO_3, $UO_2(OH)_2$, $UO_3{\cdot}2H_2O$, and $CaUO_4$ controls U aqueous concentrations. However, observed U concentrations start to decrease much earlier (at $<$30 mmol/L NaOH added or at pH $<$4.5). Both U and Tc were rapidly removed from the solution phase when addition of NaOH exceeded ~42 mmol/L (or at pH ~5.5), which coincided with the precipitation of Al and Fe hydroxides. Concentrations of U and Tc then increased slightly with further increase in pH. At pH ~8.6, ~20 and 15% of U and Tc were brought back to the solution phase, respectively.

These observations may be partially explained by the speciation of UO_2^{2+} in aqueous solutions and its sorption onto Al- and Fe-oxyhydroxide precipitates (Couston et al., 1995; Moulin et al., 1995; Duff and Amrhein, 1996; Casas et al., 1998; Moulin et al., 1998; Lenhart and Honeyman, 1999; Bargar et

al., 2000). Although UO_2^{2+} tends to hydrolyze at pH above 3.5, the dominant U(VI) species at pH <5.5 are predicted to be soluble $UO_2SO_{4,aq}$, UO_2OH^+, $(UO_2)_2(OH)_2^{2+}$, and $(UO_2)_2(OH)_5^+$ with some residual UO_2^{2+} and perhaps small quantities of $UO_2NO_3^+$ species (Couston et al., 1995; Moulin et al., 1998) because of a relatively high concentration of NO_3^- in groundwater. The formation of uranyl-carbonate species [such as UO_2CO_3 and $UO_2(CO_3)_2^{2-}$] was also likely to occur at pH ~5.5. However, the fact that more than 90% of U(VI) was precipitated or removed at pH ~5.5 (or with ~42 mmol/L NaOH added, Fig. 2d) suggests that these U(VI) species were sorbed onto and then coprecipitated with Al and Fe-oxyhydroxides. Oxide minerals, particularly Fe oxyhydroxides, are known to have high sorption capacities for uranium (Hsi and Langmuir, 1985; Duff and Amrhein, 1996; Lenhart and Honeyman, 1999; Bargar et al., 2000; Tao et al., 2000). Even at pH 4.5, Bargar et al. (2000) reported that a large percentage of U(VI) could be sorbed on hematite as monomeric hematite-U(VI)-carbonato ternary complexes. Direct surface complexation between UO_2^{2+} species and Al and Fe-oxyhydroxides and the formation of mixed hydroxide minerals could also be the mechanisms responsible for U(VI) removal. For example, Tao et al. (2000) reported that the sorption of U(VI) increased rapidly with an increase of pH from ~3 to 6, and nearly 100% of UO_2^{2+} was retained by Al and Fe oxides between pH ~6 and 10 in the absence of carbonates. Additionally, previous studies have shown that all Fe and Al-oxyhydroxides strongly sorb dissolved U(VI) species and that the amount of sorption is greatest on amorphous Fe and Al-hydroxides and least on crystalline minerals such as hematite (Langmuir, 1978; Hsi and Langmuir, 1985; Ho and Miller, 1986; Payne et al., 1994; Prikryl et al., 1994; McKinley et al., 1995). It is therefore not surprising to observe a rapid sorption and coprecipitation of U(VI) (Fig. 2d) because of a relatively high Al^{3+} content in groundwater and a massive precipitation of amorphous Al hydroxides during titration.

Little desorption or dissolution of U(VI) species were observed up to pH ~9, as was found by other investigators in the hydroxide system (Tao et al., 2000). There appeared to be a slightly increased desorption of U(VI) with an increase of pH (or addition of NaOH), and this observation may be attributed to the formation of uranyl-carbonate species at higher pHs because the experiment was not performed under CO_2-free atmosphere. However, the model also failed to describe the observed data with the consideration of the equilibrium with atmospheric CO_2 (Fig. 2d) because the model may have overestimated the carbonate activity in solution, as stated earlier.

The reaction path model did not consider Tc because TcO_4^- anion is the most stable aqueous species under oxic or suboxic conditions, and its valent state does not change with pH under given experimental conditions (Schulte and Scoppa, 1987). Its concentration profile may be simply explained by the electrostatic interactions because the zero points of charge (ZPC) of amorphous Fe and Al hydroxides are in the range of ~7.5 to 9.1 (Sposito, 1984; Green-Pedersen and Pind, 2000). In other words, net surface charge properties of solids could be responsible for the sorption of negatively charged TcO_4^- up to pH ~7.5 to 9.

3.2. Geochemical Reactions and Mineral Precipitation in Carbonate System

3.2.1. Al, Fe, and SO_4^{2-} Concentrations

As observed in the hydroxide system, addition of Na_2CO_3 resulted in the precipitation of Al and Fe hydroxide minerals with an increase of pH (Fig. 4a,b). In the first part of the titration, solution pH was largely buffered by the hydrolysis of Al (and Fe), resulting in the formation of aqueous Al or Fe-hydroxy species as well as the solid phase Al or Fe hydroxides. Most of Al was precipitated out with addition of ~20 mmol/L Na_2CO_3 (or at pH above 5). The model simulation was in good agreement with observed Al concentration profile when addition of Na_2CO_3 was <~75 mmol/L. However, the simulation deviated greatly when addition of Na_2CO_3 was >75 mmol/L as observed in the hydroxide system, in which simulated Al concentrations increased above neutral pH due to the amphoteric nature of Al and the alteration of $Al_4(OH)_{10}SO_4$ to the more soluble $Al(OH)_{3,am}$. The SO_4^{2-} concentration decreased initially (with ~20 mmol/L Na_2CO_3 added) and appeared in general agreement with the model predictions (Fig. 4a). The model did a relatively poor job in describing the precipitation behavior of Fe, which occurred at higher pH values than that predicted by the model simulation (Fig. 4b). About 30% of Fe still was left in the solution phase with the addition of ~22 mmol/L Na_2CO_3 (pH at ~5). These observations are consistent with early studies of Fe(III) hydrolysis. Hedstrom (1953) and Biedermann and Schindler (1957) found that titration of acidic Fe(III) solutions with $NaHCO_3$ resulted in solutions that were oversaturated with respect to $Fe(OH)_3$, whereas oversaturation could not be achieved when using NaOH as titrant.

3.2.2. Ca, Mg, and Mn Concentrations

As opposed to the hydroxide system, Ca^{2+} concentrations began decreasing when the addition of Na_2CO_3 exceeded ~25 mmol/L (or at pH ~5.5) because of a relatively low solubility of Ca carbonates (Figs. 4c and 1b). However, Mg^{2+} concentrations remained unchanged until ~75 mmol/L Na_2CO_3 added (or pH ~7.7). These results suggested that, in contrast to the NaOH titration, more than one solid phase would be needed to describe the Ca^{2+} and Mg^{2+} concentrations. A magnesian calcite was included for consideration in the Na_2CO_3 simulation (Table 2). The proposed composition of the solid ($Ca_{0.85}Mg_{0.15}CO_3$) was derived from inspection of the data as noted previously, and the log K for the solid was interpolated from Figure 1 of Bischoff et al. (1987). As shown in Figure 4c, the model did reasonably well in describing the concentration profiles of Ca^{2+} and Mg^{2+}.

The primary inconsistencies between simulation and observations are similar to those noted for the NaOH titration. Decreases in the concentration of Mn^{2+} were not observed until after significant loss of Ca^{2+}, suggesting that sorption or coprecipitation may be a more appropriate mechanism for Mn^{2+} loss than $MnCO_3$ precipitation alone. Most Mn^{2+} was precipitated out at pH above 7 by using Na_2CO_3 as the titration base. However, when NaOH was used for the titration, a large proportion of Mn^{2+} still was left in solution even at pH ~8,

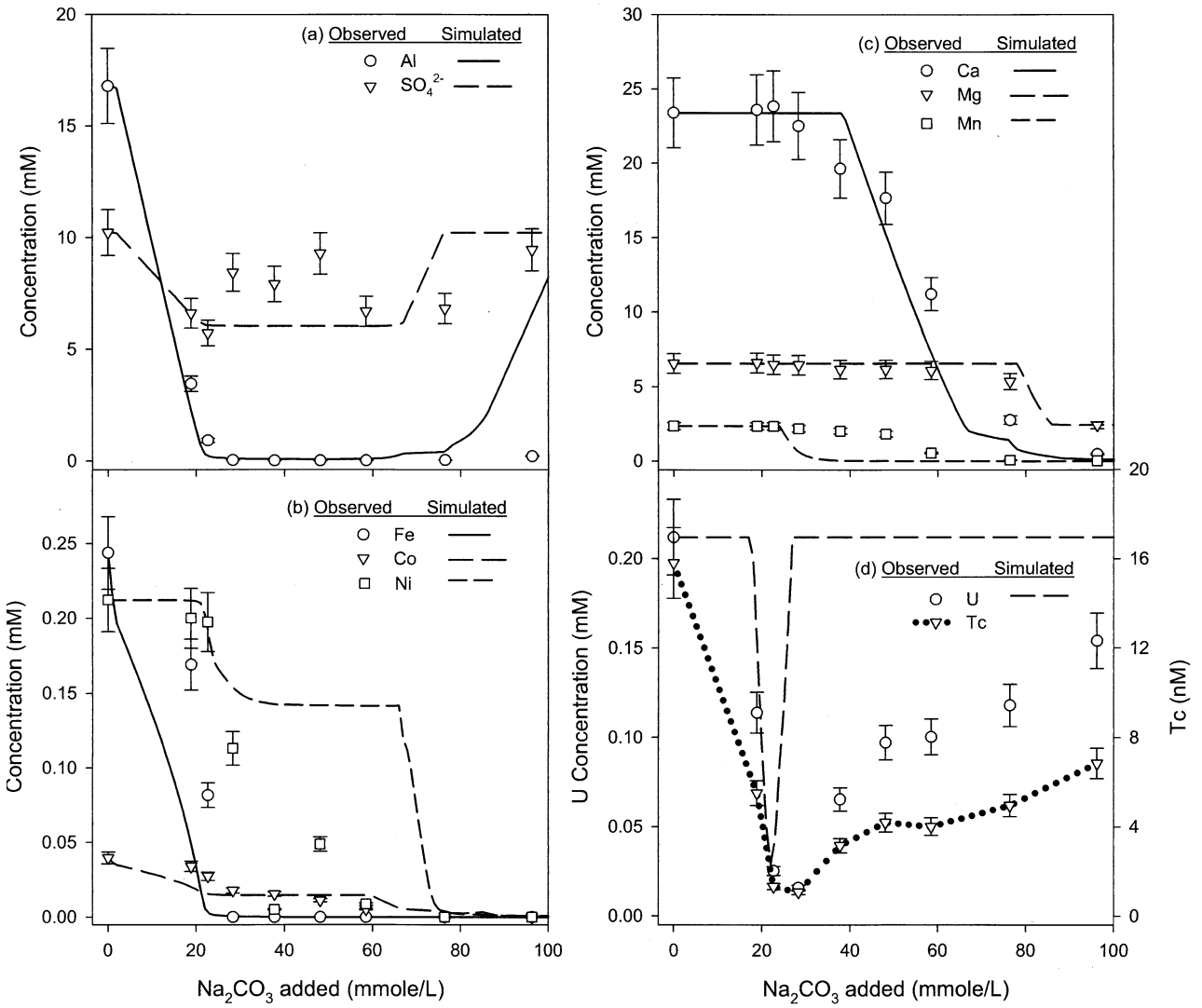

Fig. 4. Observed and simulated total concentrations of metal cations, Tc, and sulfate for the Na_2CO_3 titration of a contaminated groundwater with a low pH and high concentrations of Al and Ca. Symbols represent observed data, whereas lines are model simulations except for Tc. Error bars indicate ±10% of the observed value.

and these observations could not be explained by the solubility products of $MnCO_3$ and $Mn(OH)_2$.

3.2.3. Co and Ni Concentrations

The model described concentration profiles of Co^{2+} reasonably well (Fig. 4b), considering that solution Co^{2+} was initially controlled by the precipitation of $FeCo_{0.1}(OH)_{3.2}$ as described in the hydroxide section 3.1. Subsequent controls on Co^{2+} concentrations may be explained by the sorption onto precipitated Al- and Fe-hydroxide solids and eventually precipitation of $CoCO_3$. As indicated previously, Al-hydroxides are particularly effective in sorbing Co^{2+} by forming a double-hydroxide phase, and these colloidal precipitates or coprecipitates are highly stable in aqueous solution (Bibak et al., 1995; Towle et al., 1997).

Ni^{2+} was removed from the solution phase at pH above 5, and the model was not completely able to describe concentration profiles of Ni^{2+} for the Na_2CO_3 titration (Fig. 4b). Initial losses of Ni^{2+} were attributed to sorption onto Fe and Al solids. The extent of Ni^{2+} loss in the model is limited by the number of available sorption sites (estimated using literature values for $Fe(OH)_3$ and $Al(OH)_3$) which was invariant from 30–65 mmol/L Na_2CO_3 added. When $Al_4(OH)_{10}SO_4$ alters to $Al(OH)_3$, new sites for sorption become available and may account for the removal of the remaining Ni^{2+}. Precipitation of $Ni(OH)_2$ has only a minor impact on Ni^{2+} concentrations. The model did not include reactions for sorption or coprecipitation of Ni^{2+} onto $CaCO_3{\cdot}H_2O$. Such a mechanism may improve the match between model and observations, particularly in the pH range 5.8–7.7.

3.2.4. U and Tc Concentrations

As observed in the hydroxide system, the model was unable to adequately describe concentration profiles of U during titra-

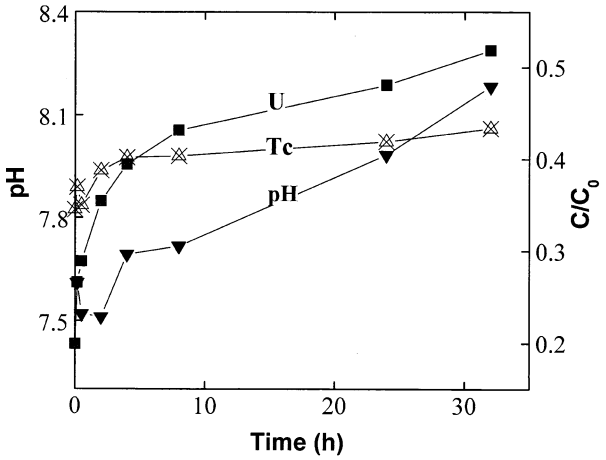

Fig. 5. The pH changes and kinetics of U and Tc desorption and/or dissolution from freshly precipitated mineral solids by rapidly mixing the groundwater with 2 mol/L Na_2CO_3 to pH ~7.5 and then leaving the suspension to reequilibrate for an extended period of time.

tion with Na_2CO_3 (Fig. 4d). At pH below ~5.5 (with addition of ~25 mmol/L Na_2CO_3), more than 90% of U was precipitated, suggesting possible precipitation or coprecipitation with Al and Fe-oxyhydroxides and/or precipitation of UO_2CO_3 species because of its relatively low solubility ($K_{sp} = 1.8 \times 10^{-12}$). The model predicted a complete resolubilization of U (as $UO_2(CO_3)^{2-}$) with further addition of Na_2CO_3 (at >22 mmol/L), which is consistent with the trend of observed data but deviated significantly from experimental observations (Fig. 4d). Results indicated that, with an increased addition of Na_2CO_3 (>25 mmol/L or at pH above ~5.5), desorption or resolubilization of U(VI) species occurred at a much slower rate than the model predicted (Fig. 4d). With the addition of ~96 mmol/L Na_2CO_3 (at pH ~9), ~70% of U was brought back to the solution phase. These observations may be partially attributed to a reduced surface complexation between U(VI)-carbonate complexes and Al or Fe hydroxides. In the carbonate system, the sorption of CO_3^{2-} onto Al and Fe-oxyhydroxides could be anticipated, which could lead to a lower mineral-oxide ZPC and thus an increased desorption of U(VI) species as pH increased. More importantly, the equilibrium U(VI) concentration was likely controlled by the aqueous carbonate species such as $UO_2(CO_3)_2^{2-}$ and $UO_2(CO_3)_3^{4-}$ because it is known that UO_2^{2+} forms strong complexes with carbonate. These reactions may have resulted in not only the dissolution of uranyl-hydroxide species but also the dissociation or desorption of uranyl-carbonate complexes from hydroxy-Al and Fe precipitates (Bargar et al., 2000).

The lack of agreement between simulation and observations also suggests the influence of kinetic constraints or the formation of poorly characterized solid solutions involving U(VI) that exert control of the concentration of this constituent. Additional analyses indicated that the dissolution or desorption of UO_2^{2+} species from freshly precipitated Al and Fe hydroxides were indeed kinetically limited. By mixing the groundwater with Na_2CO_3 to an initial pH ~7.5 in a short time (not at equilibrium), we observed that more than 80% of U was rapidly removed by the sorption or coprecipitation process (Fig. 5).

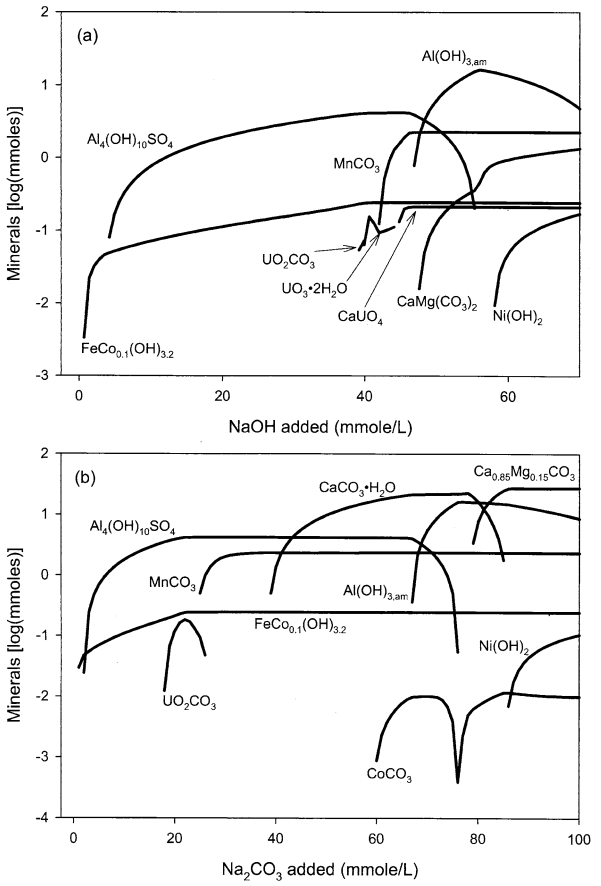

Fig. 6. Simulated mineral precipitation as a function of titrant addition with: (a) NaOH and (b) Na_2CO_3.

However, the concentration of U in solution phase increased consistently and did not reach steady state even after ~32 h of equilibration although >50% of U was redissolved. The dissolution and desorption rate appeared to be the most rapid initially (within 10 h), followed by a slow increase in solution U concentration. It is important to note that the solution pH increased with time, which may suggest a slow conversion of hydroxy-uranyl to uranyl-carbonate species as shown in the following reactions:

$$UO_2(OH)^+ + CO_3^{2-} \Leftrightarrow UO_2CO_3 + OH^-$$

$$UO_2(OH)_2 + 2CO_3^{2-} \Leftrightarrow UO_2(CO_3)_2^{2-} + 2OH^- \quad (3)$$

These reactions could result in the dissociation of hydroxy-uranyl species and the formation of soluble uranyl-carbonate species, which led to the desorption of U(VI) species. However, it is possible that the dissolution of other carbonate solids may also result in a pH increase, given the complexity of the FRC groundwater.

As opposed to that of UO_2^{2+}, the desorption of TcO_4^- appeared to be essentially time-independent, and only small variations in TcO_4^- concentrations occurred initially (~2 h) after addition of Na_2CO_3. Different mechanisms may be involved in the sorption, precipitation, and desorption of TcO_4^-. Because of the stability and high solubility of TcO_4^- anions, TcO_4^- was

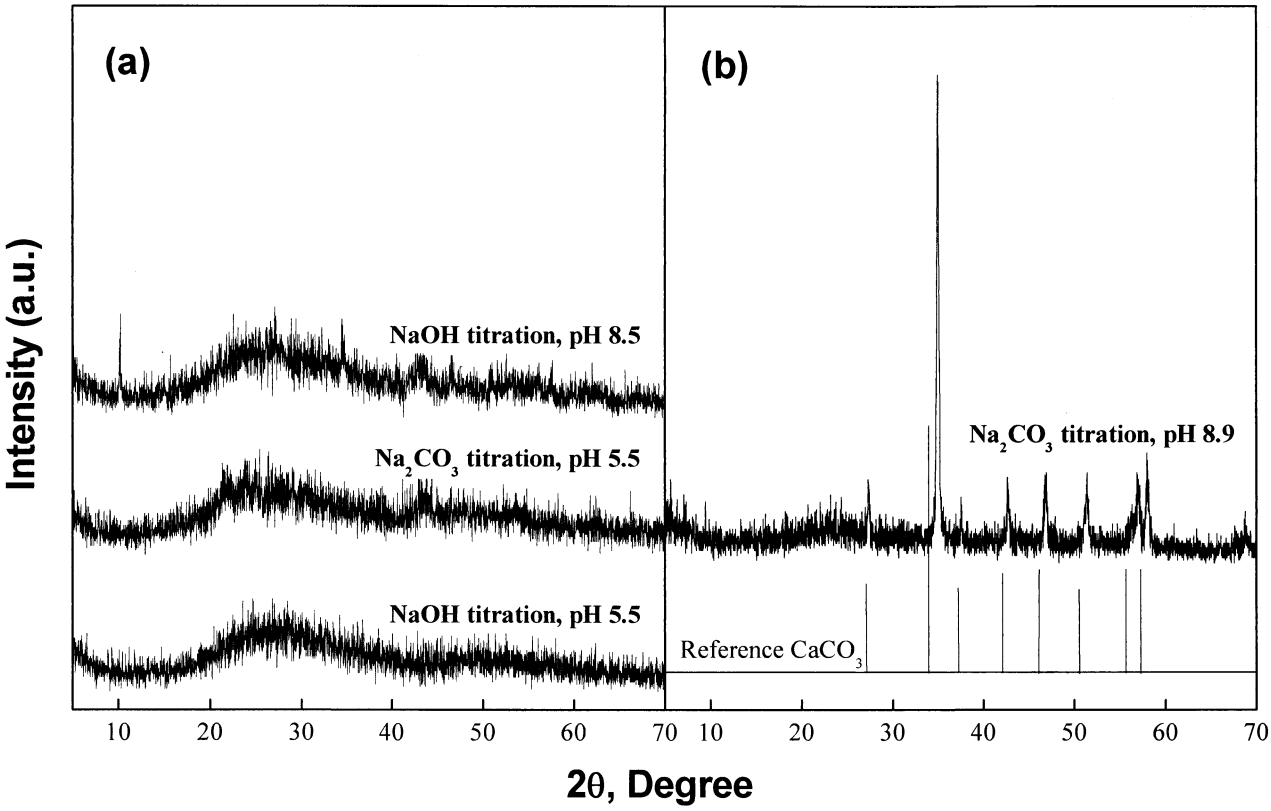

Fig. 7. X-ray diffraction analysis of air-dried mineral precipitates obtained from the titration of groundwater with: (a) NaOH to pH ~5.5 and 8.5 or Na_2CO_3 to pH ~5.5 and (b) Na_2CO_3 at pH ~8.9. The reference XRD pattern of calcite is included for comparison.

likely removed by sorption and then coprecipitation with Al and Fe oxyhydroxides, as discussed previously. In the hydroxide system (e.g., NaOH) as pH increased, an insignificant amount of TcO_4^- was desorbed from Al and Fe oxyhydroxides within the pH range studied (Fig. 2d). This observation could be explained by the fact that both Al and Fe oxyhydroxides were still positively charged (assuming a ZPC of ~7.5 to 9). However, in the carbonate system, ~40% of Tc was desorbed or redissolved at pH ~9, which was slightly lower than that observed for UO_2^{2+} desorption. Unlike UO_2^{2+}, pertechnetate anions do not form carbonate species (Schulte and Scoppa, 1987). However, carbonates could possibly invoke a specific modification to the surface of Al and Fe hydroxides and thus restrict TcO_4^- sorption. More specifically, specific sorption of CO_3^{2-} species on Al- and Fe-hydroxide surfaces may have resulted in a decreased surface charge and a downward shift in the ZPC of Al and Fe hydroxides (Mukhopadhyay and Walther, 2001). It is therefore not a simple electrostatic interaction or competition between added CO_3^{2-} and TcO_4^- anions because of the presence of high concentrations of NO_3^- and SO_4^{2-} (which would otherwise also compete with the sorption of TcO_4^- in both NaOH and Na_2CO_3 systems). Note that molar concentrations of NO_3^- and SO_4^{2-} were ~6–7 orders of magnitude higher than that of TcO_4^- in groundwater (Table 1). Apparently, there is an extremely high affinity for TcO_4^- to be sorbed onto Al and Fe hydroxides perhaps by forming inner-sphere surface complexes. These observations are supported by the fact that TcO_4^- is a large, poorly hydrated anion and has a natural tendency to be strongly sorbed by a variety of adsorbents (Wildung et al., 1986; Schulte and Scoppa, 1987; Schwochau and Pleger, 1993).

3.3. Solid-phase Precipitates and Characterization

The anticipated solid-phase mineral precipitates during titration were also analyzed by the geochemical process modeling (Fig. 6a,b) and the laboratory analyses of some selected samples. As indicated previously, in the hydroxide system, solution pH was initially buffered by the hydrolysis of Fe and Al resulting in the formation of aqueous hydrolysis species as well as the solid-phase precipitates $FeCo_{0.1}(OH)_{3.2}$ and $Al_4(OH)_{10}SO_4$ (Fig. 6a). After most of the Fe and Al had been precipitated from solution, the pH showed a steep increase with minor buffering accompanying the precipitation of $MnCO_3$ (Fig. 1a). At pH ~7.7 the expected alteration of $Al_4(OH)_{10}SO_4$ to $Al(OH)_{3,am}$ releases protons to solution according to the reaction in Eqn. 4 below, conferring additional buffering capacity. As the amount of titrant added exceeds 55 mmol/L NaOH, the pH is buffered by precipitation or coprecipitation of a disordered dolomite, $CaMg(CO_3)_2$. The model also predicted the precipitation of UO_2CO_3, $UO_3 \cdot 2H_2O$, $CaUO_4$, and $Ni(OH)_2$ minerals (Fig. 6a) although these minerals do not confer significant buffering capacity of the system because of their low concentrations in groundwater.

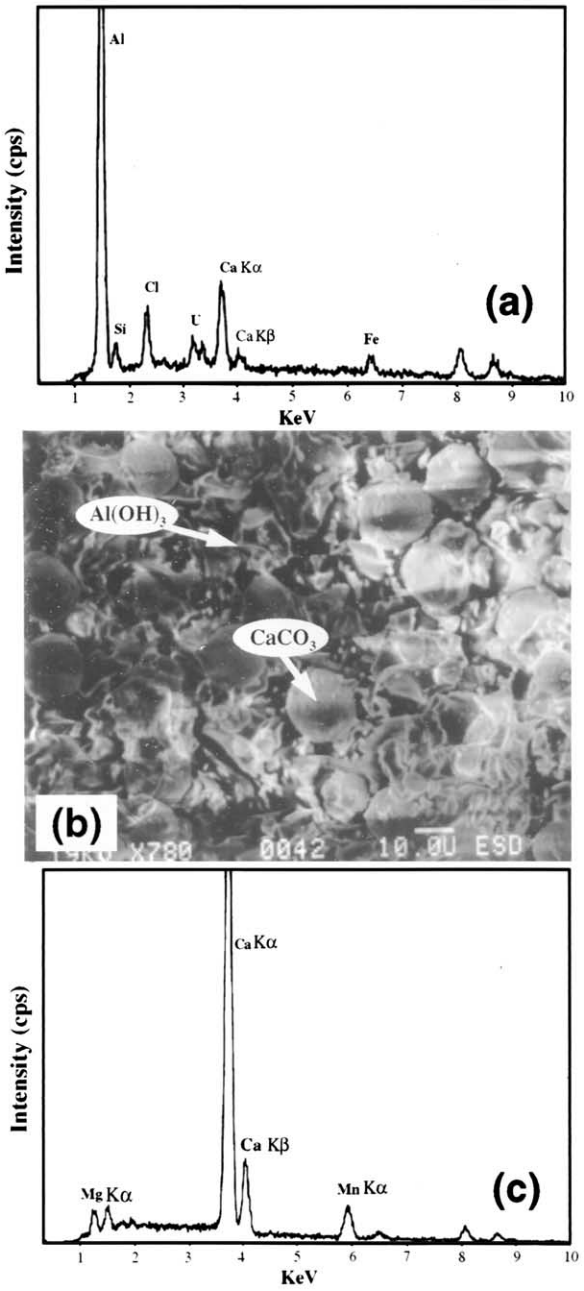

Fig. 8. (a) Energy dispersive X-ray (EDX) analysis of precipitated solids at pH ~5.5; (b) SEM image of precipitated carbonate minerals (as spherical-shaped crystals) and hydroxy-Al and Fe precipitates at pH ~9; and (c) EDX analysis of spherically shaped mineral precipitates using Na_2CO_3 as a titrant.

$$Al_4(OH)_{10}SO_4 + 2H_2O \rightarrow 4Al(OH)_{3,am} + SO_4^{2-} + 2H^+ \quad (4)$$

Similarly in the carbonate system (Fig. 6b), the solution pH was initially buffered primarily by hydrolysis reactions of Al and Fe, followed by the dominant buffering reactions or the precipitation of $MnCO_3$, $CaCO_3 \cdot H_2O$, and the alteration of $Al_4(OH)_{10}SO_4$ to $Al(OH)_{3,am}$ (Eqn. 4). Again, since U, Co, and Ni are minor components of the system, their precipitation such as $CoCO_3$, UO_2CO_3, and $Ni(OH)_2$ do not confer significant impact to overall pH changes with addition of either NaOH or Na_2CO_3. As discussed previously, the model nevertheless did a poor job in describing the equilibrium U concentration and its mineral precipitation (Fig. 6b).

Most minerals discussed above (Fig. 6a,b) could not be identified within the XRD detection limit partly because of the fact that they are only the minor components of the precipitated solids as compared with those of Al and Ca (Table 1). Additionally, with the exception of $CaCO_3$, all solid precipitates appeared to be amorphous in nature despite the fact that they were air-dried for about a week before the analysis (Fig. 7a,b). As indicated earlier, these amorphous Al and Fe oxyhydroxides are perhaps largely responsible for the sorption and/or coprecipitation of U(VI), Tc(VII), and other metal cations during titration. The SEM-EDX analyses revealed that U(VI) was indeed sorbed and/or coprecipitated with the hydroxy-Al and Fe precipitates at pH ~5.5 when Na_2CO_3 was used as the titrant (Fig. 8a). Other constituents such as Tc, Co, and Ni could not be observed (Fig. 8a) largely because of their low concentrations in the groundwater.

With further addition of base (Na_2CO_3) to pH ~9, most Ca and Mn were precipitated out as discussed earlier. The SEM and EDX analyses showed that these carbonate precipitates formed separate phases from those of hydroxy-Al and Fe precipitates (Fig. 8b). Those spherically shaped solid precipitates were identified primarily as $CaCO_3$ with minor components being Mg and Mn. No Al, Fe, or U were identified in these carbonate precipitates (Fig. 8c), and these observations are therefore consistent with the concentration profiles as shown in Figures 2 and 4. Additionally, a careful examination of the XRD data indicated that some isomorphic substitution had occurred among Ca, Mg, or Mn, because the XRD pattern of the carbonate precipitates shifted slightly and did not exactly match with that of calcite ($CaCO_3$) (Fig. 7b). These results provide strong evidences of the formation of mixed minerals such as magnesian calcite or the coprecipitation of Ca, Mn, and Mg carbonates, given the complexity of this FRC groundwater. Previous studies (Goldsmith and Graf, 1957, 1960) also indicated that isomorphic substitutions are common in solid solutions, most frequently being those involving replacement of Ca by Mg and/or Mn.

4. CONCLUSIONS

This study concludes that, although the hydrolysis and precipitation of a single metal cation are known, complex reactions such as sorption/desorption and coprecipitation/dissolution could occur simultaneously and be kinetically limited during titration of groundwater with multiple cationic and anionic species and a wide range of concentrations. The geochemical reaction path modeling could be useful for predicting the concentration profiles of aqueous species, solution pH, and mineral precipitates. However, careful considerations must be given to the speciation, sorption, and coprecipitation processes as well as the kinetics of the desorption and dissolution to better describe the concentration profiles of U and Tc. Sorption and coprecipitation of U and Tc with amorphous Al and Fe oxyhydroxides were likely the major mechanisms responsible for their removal at pH below ~5.5, but desorption or dissolution

of U and Tc occurred at higher pH values in the presence of carbonates. Results also suggest the formation of mixed mineral phases such as Ca, Mg, Mn carbonates and double hydroxide solids of Ni and Co with Al and Fe oxyhydroxides, although detailed micro- and spectroscopic studies are needed to further validate their formations and structural properties. Nevertheless, this study may shed additional light for improved design of a successful remediation strategy and in the prediction of metal/radionuclide activities at pre- and posttreatment conditions. Additionally, the present study may point out an alternative potential remediation strategy to remove U and Tc by a partial neutralization of the contaminated groundwater with hydroxides or carbonates at this particular site.

Acknowledgments—Technical assistance provided by Ms. Y. K. Ku and T. L. Mehlhorn is gratefully appreciated. Funding for this research was provided by the Office of Science Biological and Environmental Research, the Natural and Accelerated Bioremediation Research (NABIR) Program, U.S. Department of Energy under contract DE-AC05-00OR22725 with Oak Ridge National Laboratory, which is managed by UT-Battelle, LLC.

Associate editor: D. Sparks

REFERENCES

Adams F. and Hajek B. F. (1978) Effects of solution sulfate, hydroxide, and potassium concentrations on the crystallization of alunite, basaluminite, and gibbsite from dilute aluminum sulfate solutions. *Soil Sci.* **126,** 169–173.

Adams F. and Rawajfih Z. (1977) Basaluminite and alunite: A possible cause of sulfate retention by acid soils. *Soil Sci. Soc. Am. J.* **41,** 686–692.

Baes C. F. and Mesmer R. E. (1976) The Hydrolysis of Cations. John Wiley & Sons.

Bargar J. R., Reitmeyer R., Lenhart J. J., and Davis J. A. (2000) Characterization of U(VI)-carbonato ternary complexes on hematite: EXAFS and electrophoretic mobility measurements. *Geochim. Cosmochim. Acta* **64**(16), 2737–2749.

Bethke C. M. (2001) *The Geochemist's Workbench. Users Guide*. University of Illinois p. 224.

Bibak A., Moberg J. P., and Borggaard O. K. (1995) Cobalt retention by Danish spodosol samples in relation to contents of organic-matter and aluminum, iron and manganese oxides. *Acta Agric. Scand. Sect. B-Soil. Plant Sci.* **45**(3), 0153–0158.

Biedermann G. and Schindler P. (1957) On the solubility product of precipitated iron(III) hydroxide. *Acta Chem. Scand.* **11,** 731–740.

Bischoff W. D., Mackenzie F. T., and Bishop F. C. (1987) Stabilities of synthetic magnesian calcites in aqueous solution: Comparison with biogenic materials. *Geochim. Cosmochim. Acta* **51,** 1413–1423.

Brina R. and Miller A. G. (1992) Direct detection of trace levels of uranium by laser-induced kinetics phosphorimetry. *Anal. Chem.* **64,** 1413–1418.

Carroll-Webb S. and Walther J. V. (1988) A surface complex reaction model for the pH-dependence of corundum and kaolinite dissolution. *Geochim. Cosmochim. Acta* **52,** 2609–2623.

Casas I., De Pablo J., Gimenez J., Torrero M. E., Bruno J., Cera E., Finch R. J., and Ewing R. C. (1998) The role of pe, pH, and carbonate on the solubility of UO_2 and uraninite under nominally reducing conditions. *Geochim. Cosmochim. Acta* **62,** 2223–2231.

Cook P. G., Solomon D. K., Sanford W. E., Busenberg E., Plummer L. N., and Poreda R. J. (1996) Inferring shallow groundwater flow in saprolite and fractured rock using environmental tracers. *Wat. Res.* **32,** 1501–1509.

Couston L., Pouyat D., Moulin C., and Decambox P. (1995) Speciation of uranyl species in nitric acid medium by time-resolved laser-induced fluorescence. *Appl. Spectr.* **49**(3), 349–353.

Delany J. M, and Lundeen S. R (1990) The LLNL thermochemical database. *Lawrence Livermore National Laboratory Report UCRL-21658.* p. 150.

Duff M. C. and Amrhein C. (1996) Uranium(VI) adsorption on goethite and soil in carbonate solutions. *Soil Sci. Soc. Am. J.* **60,** 1393–1397.

Dzombak D. A. and Morel F. M. M. (1990) *Surface Complexation Modeling: Hydrous Ferric Oxide.* Wiley.

Fredrickson J. and Gorby A. (1996) Environmental processes mediated by iron-reducing bacteria. *Current Opin. Biotechnol.* **7,** 287–294.

Fredrickson J. K., Kostandarithes H. M., Li S. W., Plymale A. E., and Daly M. J. (2000) Reduction of Fe(III), Cr(VI), U(VI), and Tc(VII) by Deinococcus radiodurans R1. *Appl. Environ. Microbiol.* **66**(5), 2006–2011.

Goldsmith J. R. and Graf D. L. (1957) The system CaO-MnO-CO_2: Solid solution and decomposition relations. *Geochim. Cosmochim. Acta* **11,** 310–334.

Goldsmith J. R. and Graf D. L. (1960) Subsolids relations in the system $CaCO_3$-$MgCO_3$-$MnCO_3$. *J. Geol.* **68,** 324–335.

Green-Pedersen H. and Pind N. (2000) Preparation, characterization, and sorption properties for Ni(II) of iron oxyhydroxide-montmorillonite. *Coll. Surf. A-Phys. Eng. Aspects* **168**(2), 133–145.

Grenthe I., Fuger J., Konings R. J. M., Lemire R. J., Muller A. B., Cregu C. N. T., and Wanner H. (1992) *Chemical Thermodynamics of Uranium.* North-Holland. p. 715.

Gu B., Brown G. M., Bonnesen P. V., Liang L., Moyer B. A., Ober R., and Alexandratos S. D. (2000) Development of novel bifunctional anion-exchange resins with improved selectivity for pertechnetate sorption from contaminated groundwater. *Environ. Sci. Technol.* **34,** 1075–1080.

Gu B., Liang L., Dickey M. J., Yin X., and Dai S. (1998) Reductive precipitation of uranium(VI) by zero-valence iron. *Environ. Sci. Technol.* **32,** 3366–3373.

Gu B., Watson D. B., Phillips D. H., and Liang L. (2002) Biogeochemical, mineralogical, and hydrological characteristics of an iron reactive barrier used for treatment of uranium and nitrate. In *Groundwater Remediation of Trace Metals, Radionuclides, and Nutrients, With Permeable Reactive Barriers* (eds. D. L. Naftz, S. J. Morrison, J. A. Davis, and C. C. Fuller), pp. 305–342. Academic Press.

Hedstrom B. O. A. (1953) Studies on the hydrolysis of metal ions VII. The hydrolysis of the iron(III) ion, Fe^{3+}. *Arkiv för Kemi.* **6,** 1–16.

Ho C. H. and Miller N. H. (1986) Adsorption of uranyl species from bicarbonate solution onto hematite particles. *J. Coll. Interf. Sci.* **110,** 165.

Hsi C. K. D. and Langmuir D. (1985) Adsorption of uranyl onto ferric oxyhydroxides: Application of the surface complexation site-binding model. *Geochim. Cosmochim. Acta* **49,** 1931–1941.

Hull H. and Turnbull A. G. (1973) A thermochemical study of monohydrocalcite. *Geochim. Cosmochim. Acta* **37,** 685–694.

Kaminski R., Purcell F. J., and Russavage E. (1981) Uranyl phosphorescence at the parts-per-trillion level. *Anal. Chem.* **53,** 1093–1096.

Langmuir D. (1978) Uranium solution-mineral equilibria at low temperatures with applications to sedimentary ore deposit. *Geochim. Cosmochim. Acta* **42,** 547.

Lenhart J. J. and Honeyman B. D. (1999) U(VI) sorption to hematite in the presence of humic acid. *Geochim. Cosmochim. Acta* **63**(6), 2891–2901.

Lovley D. R. (1995) Bioremediation of organic and metal contaminants with dissimilatory metal reduction. *J. Ind. Microbiol.* **14**(2), 85–93.

McKinley J. P., Zachara J. M., Smith S. C., and Turner G. D. (1995) The influence of uranyl hydrolysis and multiple site-binding reactions on adsorption of U(VI) to montmorillonite. *Clays and Clay Minerals* **43,** 586–598.

Moulin C., Decambox P., and Decaillon J. G. (1995) Uranium speciation in solution by time-resolved laser-induced fluorescence. *Anal. Chem.* **67,** 348.

Moulin C., Laszak I., Moulin V., and Tondre C. (1998) Time-resolved laser-induced fluorescence as a unique tool for low-level uranium speciation. *Appl. Spectr.* **52,** 528–535.

Mukhopadhyay B. and Walther J. V. (2001) Acid-base chemistry of albite surfaces in aqueous solutions at standard temperature and pressure. *Chem. Geol.* **174,** 415–443.

Nordstrom D. K. (1982) The effect of sulfate on aluminum concentrations in natural waters: Some stability relations in the system Al_2O_3-SO_3-H_2O at 298K. *Geochim. Cosmochim. Acta* **46,** 681–692.

Nordstrom D. K., Plummer L. N., Langmuir D., Busenberg E., May H. M., Jones B. F., and Parkhurst D. L. (1990) Revised chemical equilibrium data for major water-mineral reactions and their limitations. In *Chemical Modeling of Aqueous Systems II* (eds. D. C. Melchior and R. L. Bassett), pp. 398–413. ACS Symposium Series 416.

Payne T. E., Davis J. A., and Waite T. D. (1994) Uranium retention by weathered schists—the role of iron minerals. *Radiochim. Acta* **66/67,** 297–303.

Plummer L. N. and MacKenzie F. T. (1974) Predicting mineral solubility from rate data: Application to the dissolution of magnesian calcite. *Am. J. Sci.* **274,** 61–83.

Prikryl J. D., Pabalan R. T., Turner D. R., and Leslie B. W. (1994) Uranium sorption on α-alumina: Effects of pH and surface-area/solution-volume ratio. *Radiochim. Acta* **66/67,** 291–296.

Roberson E. C, Hem J. D (1969) Solubility of aluminum in the presence of hydroxide, fluoride, and sulfate. *U. S. Geological Survey Water-Supply Paper 1827-C.* 37.

SAIC. (1997) Phase I report on the Bear Creek Valley Treatability study, Oak Ridge Y-12 Plant, Oak Ridge, Tennessee. Y/ER-285 Science Applications International Corporation, Oak Ridge, TN 37831.

Scheckel K. G., Scheinost A. C., Ford R. G., and Sparks D. L. (2000) Stability of layered Ni hydroxide surface precipitates: A dissolution kinetics study. *Geochim. Cosmochim. Acta* **64**(16), 2727–2735.

Scheidegger A. M., Lamble G. M., and Sparks D. L. (1997) Spectroscopic evidence for the formation of mixed-cation hydroxide phases upon metal sorption on clays and aluminum-oxides. *J. Coll. Interf. Sci.* **186**(1), 118–128.

Scheidegger A. M., Strawn D. G., Lamble G. M., and Sparks D. L. (1998) The kinetics of mixed Ni-Al hydroxide formation on clay and aluminum oxide minerals: A time-resolved XAFS study. *Geochim. Cosmochim. Acta* **62,** 2233–2245.

Schulte E. H. and Scoppa P. (1987) Sources and behavior of technetium in the environment. *Sci. Total Environ.* **64,** 163–179.

Schwochau K. and Pleger U. (1993) Basic coordination chemistry of technetium. *Radiochim. Acta* **63,** 103–110.

Sposito G. (1984) *The Surface Chemistry of Soils*. Oxford University Press, New York.

Sverjensky D. A. (1984) Prediction of Gibbs free energies of calcite type carbonates and the equilibrium distribution of trace elements between carbonates and aqueous solutions. *Geochim. Cosmochim. Acta* **48,** 1127–1134.

Tao Z. Y., Chu T. W., Du J. Z., Dai X. X., and Gu Y. J. (2000) Effect of fulvic acids on sorption of U(VI), Zn, Yb, I, and Se(IV) onto oxides of aluminum, iron, and silicon. *Appl. Geochem.* **15,** 145–151.

Thompson H. A., Parks G. A., and E. B. J. G. (1999) Dynamic interactions of dissolution, surface adsorption, and precipitation in an aging cobalt(II)-clay-water system. *Geochim. Cosmochim. Acta* **63**, 1767 –1779.

Ticknor K. V. (1994) Sorption of nickel on geological materials. *Radiochim. Acta* **66–67,** 341–348.

Towle S. N., Bargar J. R., Brown G. E., and Parks G. A. (1997) Surface precipitation of Co(II)(aq) on Al_2O_3. *J. Coll. Interf. Sci.* **187**(1), 62–82.

Wagman D. D., Evans W. H., Parker V. B., Schumm R. H., Halow I., Bailey S. M., Churney K. L., and Nuttall R. L. (1982) The NBS tables of chemical thermodynamic properties, selected values for inorganic and C1 and C2 organic substances in SI units. *J. Phys. Chem. Ref. Data* **11**(2), 392.

Wildung R. E., Garland T. R., McFadden K. M., and Cowan C. E. (1986) *Technetium Sorption in Surface Soils.* Elsevier Appl. Sci. Publishers.

Wildung R. E., Gorby Y. A., Krupka K. M., Hess N. J., Li S. W., Plymale A. E., McKinley J. P., and Fredrickson J. K. (2000) Effect of electron donor and solution chemistry on products of dissimilatory reduction of technetium by *Shewanella putrefaciens*. *Appl. Environ. Microbiol.* **66,** 2451–2460.

Zachara J. M., Cowan C. E., and Resch C. T. (1991) Sorption of divalent metals on calcite. *Geochim. Cosmochim. Acta* **55,** 1549–1562.